

Effect of inter-system crossing rates and optical illumination on the polarization of nuclear spins nearby nitrogen-vacancy centers

H. Duarte,^{1,2} H. T. Dinani,^{1,3} V. Jacques,⁴ and J. R. Maze^{1,5}

¹*Facultad de Física, Pontificia Universidad Católica de Chile, Santiago 7820436, Chile*

²*Faculty of Physics, Universidad Técnica Federico Santa María,
Avda. Vicuña Mackenna 3939, Santiago, Chile*

³*Centro de Investigación DAiTA Lab, Facultad de Estudios Interdisciplinarios,
Universidad Mayor, Santiago, Chile*

⁴*Laboratoire de Charles Coulomb, University of Montpellier*

⁵*Research Centre for Nanotechnology and Advanced Materials,
Pontificia Universidad Católica de Chile, Santiago, Chile*

(Dated: December 22, 2024)

Several efforts have been made to polarize the nearby nuclear environment of nitrogen-vacancy (NV) centers for quantum metrology and quantum information applications. Different methods showed different nuclear spin polarization efficiencies and rely on electronic spin polarization associated to the NV center, which in turn crucially depends on the inter-system crossing. Recently, the rates involved in the inter-system crossing have been measured leading to different transition rate models. Here, we consider the effect of these rates on several nuclear polarization methods based on the level anti-crossing, and precession of the nuclear population while the electronic spin is in the $m_s = 0$ and $m_s = 1$ spin states. We show that the nuclear polarization depends on the power of optical excitation used to polarize the electronic spin. The degree of nuclear spin polarization is different for each transition rate model. Therefore the results presented here are relevant for validating these models and for polarizing nuclear spins. Furthermore, we analyze the performance of each method by considering the nuclear position relative to the symmetry axis of the NV center.

I. INTRODUCTION

Nuclear spins, due to their isolation, have very long coherence times and hence are promising candidates for storing and processing quantum information [1, 2]. For such applications, the state of nuclear spins should be initialized and read out with high fidelity. However, this is difficult due to the small magnetic moment of nuclear spins. In some cases, nuclear spins can be accessed through an ancillary electronic spin. For instance, nuclear spins of carbon (^{13}C with spin $1/2$) and nitrogen (^{14}N with spin 1 or ^{15}N with spin $1/2$) in diamond are accessible through the ancillary electron spin of the nitrogen-vacancy (NV) center [3, 4]. Therefore, understanding the dynamics of the electronic spin is crucial for implementing nuclear spin polarization protocols.

The electronic spin of NV centers have been widely used in quantum metrology and quantum information processing [5–9] due to its long coherence time in a wide range of temperatures, and its accessibility through optical excitation [10, 11]. The read-out of the electronic spin of the NV center by optical excitation is a result of a spin-dependent inter-

system crossing involving metastable singlet states [12]. Although several models have been proposed to describe the optical excitation of the center and transitions to and from the singlet states [13–17], it is still not clear which model is valid, and they have a significant impact on the polarization of nearby nuclear spins.

One of the widely used methods to polarize nuclear spins consists of transferring the electron spin polarization to the nuclear spin [4, 19–21]. This is achieved, for instance, in the excited state level anti-crossing (ESLAC) [4], ground state level anti-crossing (GSLAC) [19], or via precession of nuclear spin while the electron spin is in its $m_s = 0$ [20] or $m_s = 1$ spin projections [21–23]. These methods are all based on optical excitation of the electronic spin. Therefore, the model used to describe the inter-system crossing can significantly affect the polarization of nuclear spins.

Here, we investigate how four different transition rate models [13–16] impact the polarization of nuclear spins nearby the NV center. This work is organized as follows. Section II analyzes the effect of different transition rate models on the degree of polarization of the electronic spin. Section III de-

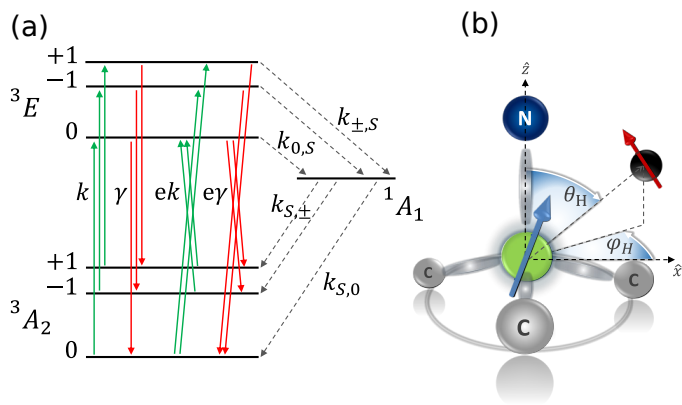


FIG. 1. (a) Schematic representation of the 7 level model used in this study showing transition rates associated to the optical excitation (k , green arrows), spontaneous decay (γ , red arrows), crossing transitions due to spin mixing (ek and $e\gamma$), and inter-system crossing transitions (dashed arrows). (b) Atomic configuration of the nitrogen-vacancy center representing the electronic spin (blue arrow) and a nuclear spin (red arrow), making a polar angle θ_H relative to the NV axis, z axis, and an azimuthal angle φ_H with respect to the x axis which is in the plane that contains the NV and one of the three carbon atoms adjacent to the vacancy.

describes three different methods for achieving nuclear spin polarization. Special attention is taken on the role of the electronic spin on the nuclear polarization dynamics for each method. Sections IV A and IV B discuss the nuclear spin polarization efficiency under different optical powers and polar position of the nuclear spin relative to the NV symmetry axis, respectively.

II. ELECTRONIC SPIN POLARIZATION

The current understanding for the electronic spin polarization of NV centers in diamond is that upon optical illumination the electronic spin can be predominantly pumped into the $m_s = 0$ state. Initially, it was proposed that only the electron in its $m_s = \pm 1$ spin projections undergoes an inter-system crossing by transiting from the excited state ${}^3E(ae)$ with spin projections $m_s = \pm 1$ to the singlet ${}^1A_1(e^2)$ and from this singlet to the ground state ${}^3A_2(e^2)$ with spin projection $m_s = 0$ [13]. We denote these transitions by the rates $k_{\pm,s}$ and $k_{s,0}$, respectively (see Fig. 1). As the optical transitions are mostly spin conserving, an almost perfect polarization of the electronic spin in the $m_s = 0$ state is

achieved after few optical cycles.

However, recent experiments have shown that additional rates must be included in the inter-system crossing [14–17]. Those experiments showed that electrons with spin projection $m_s = 0$ on the excited state can also undergo the inter-system crossing with the rate $k_{0,s}$. In addition, and more crucially, electrons can also relax from the singlet to the $m_s = \pm 1$ spin projections with $k_{s,\pm}$ rates. This has important consequences on the electronic spin polarization, especially at large optical powers.

In addition to the inter-system crossing rates, non-spin preserving optical transitions exist due to spin mixing caused by an intrinsic spin-spin interaction and magnetic field components perpendicular to the NV axis. We model the effect of the intrinsic mixing with parameter e (see Fig. 1) while the spin mixing caused by magnetic fields can be modeled separately. This spin mixing increases the population of the singlet state, especially at large optical powers, as the singlet population relaxes to the ground state at a rate about 30 times smaller than the spontaneous decay rate, denoted by γ .

The models under consideration are summarized in Table I. Model 1, adapted from Ref. [13], has no transition rate from the singlet to $m_s = \pm 1$ ground states ($k_{s,\pm} = 0$). Therefore, as the optical excitation rate, labeled by k , increases, so does the electronic spin polarization (see Fig. 2). However, models 2, 3 and 4, adapted from Refs. [14], [15] and [16], respectively, have $k_{s,\pm} \neq 0$ with model 4 having the largest rate. For these three models, the electronic spin polarization decreases as the optical excitation rate k increases. Figure 2 also shows the singlet population for all models after $2 \mu s$ of optical excitation. Transitions from excited states to the singlet populates the singlet state, which increases with optical excitation rate. Therefore, the electronic spin polarization onto $m_s = 0$ predominantly depends on the rate between k_{s0} and $k_{s\pm 1}$, i.e. on $k_{s0}/(k_{s0} + k_{s\pm 1})$.

In the following section, we discuss how these transition rate models affect the nuclear spin polarization for several polarization methods.

III. NUCLEAR SPIN POLARIZATION METHODS

Nuclear spin can be polarized using the hyperfine interaction between the electronic and nuclear spins in several ways. The Hamiltonian for an NV

TABLE I. Transition rates, based on Refs. [13–16], for the spontaneous decay γ and inter-system crossing from different spin projections of the excited state to the single, $k_{m_s, S}$, and from the singlet to the ground state spin projections, k_{S, m_s} . The parameter e is used to allow for optical transitions that do not preserve spin. See also Fig. 1.

	Model 1 [13]	Model 2 [14]	Model 3 [15]	Model 4 [16]
γ (MHz)	77	64.4	67.7	66.08
e	0.0195	0.01	0	0
$k_{0, S}$ (MHz)	0	10.6	6.4	11.1
$k_{\pm, S}$ (MHz)	30	79.8	50.7	91.9
$k_{S, 0}$ (MHz)	3.3	3	0.7	4.9
$k_{S, \pm}$ (MHz)	0	1.305	0.6	2.03

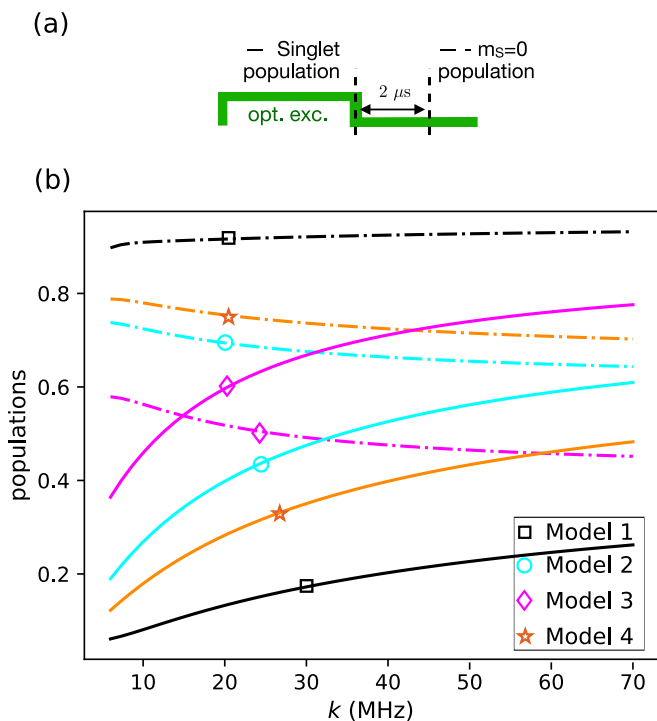


FIG. 2. (a) The sequence for calculating the population of the singlet and the $m_s = 0$ ground state of the electronic spin of the NV center. The singlet population is calculated after 2 μ s of optical excitation. The $m_s = 0$ population is calculated after 2 μ s waiting time after the optical excitation in order to let the singlet population relax to the ground state. (b) The singlet population (solid lines) and the $m_s = 0$ ground state population (dash-dotted lines) as a function of the optical excitation rate, k , for the models given in Table I.

electronic spin and a nuclear spin 1/2 is given by

$$H_i = D_i S_z^2 + \gamma_{el} \mathbf{B} \cdot \mathbf{S} + \gamma_n \mathbf{B} \cdot \mathbf{I} + H_{i, hf} \quad (1)$$

where $i = g, e$ denotes the ground and excited electronic states. The zero field splitting between the $m_s = 0$ and $m_s = \pm 1$ spin states in the ground and excited state are, $D_g = 2.87$ GHz and

$D_e = 1.42$ GHz, respectively. The electronic gyromagnetic ratio is $\gamma_{el} = 2.8$ MHz/G which is the same for ground and excited state [24]. The second and third terms are the electronic and nuclear Zeeman interactions, respectively. The gyromagnetic ratio of ^{13}C , ^{14}N and ^{15}N nuclear spins, γ_n , are 1.07 kHz/G, 0.3077 kHz/G, and -0.4316 kHz/G, respectively. The fourth term is the hyperfine interaction Hamiltonian given by

$$H_{i, hf} = A_{zz}^{(i)} S_z I_z \quad (2)$$

$$+ \frac{A_{\perp}^{(i)}}{4} (S_+ I_- + S_- I_+)$$

$$+ \frac{A'_{\perp}^{(i)}}{4} (S_+ I_+ e^{-2i\varphi_H} + S_- I_- e^{2i\varphi_H})$$

$$+ \frac{A_{\text{ani}}^{(i)}}{2} [(S_+ I_z + S_z I_+) e^{-i\varphi_H}$$

$$+ (S_- I_z + S_z I_-) e^{i\varphi_H}].$$

It is through this hyperfine interaction and the inter-system crossing mechanism that the nuclear spin can be polarized from thermal equilibrium. The first term of this Hamiltonian can be considered as an energy shift of the electronic spin depending on the nuclear spin state. The second term causes spin flip-flops between the electronic and nuclear spins when this process nearly preserves energy. The third term represents non-energy preserving spin flips. The last term represents rotation of either the electron or the nuclear spin without rotating the other spin. Note that the angle φ_H is the azimuthal angle of the nuclear spin with respect to the x axis which is in the plane that contains the NV and one of the three carbon atoms adjacent to the vacancy (see Fig. 1(b)). Some of these terms can lead to nuclear spin polarization depending on the external optical excitation, the external magnetic field and state of the electronic spin.

The hyperfine parameters in Eq. (2) depend on the relative position between the electronic and nuclear spins as follows

$$A_{zz}^{(i)} = A_c - A_d(1 - 3\cos^2\theta_H), \quad (3)$$

$$A_{\perp}^{(i)} = 2A_c + A_d(1 - 3\cos^2\theta_H), \quad (4)$$

$$A_{\text{ani}}^{(i)} = 3A_d \cos\theta_H \sin\theta_H, \quad (5)$$

$$A'_{\perp}{}^{(i)} = 3A_d \sin^2\theta_H. \quad (6)$$

Here, A_c is the contact term contribution which decays exponentially with distance between the electron and nuclear spins, A_d is the dipole-dipole hyperfine coupling, decaying as $1/r^3$ for far nuclear spins [25, 26], and θ_H is the polar angle of the nuclear spin relative to the NV axis (see Fig. 1(b)). Note that the hyperfine matrix is different for the ground and excited electronic states, denoted by i . It is straightforward to obtain the hyperfine Hamiltonian, given in Eq. (2), from a description in Cartesian coordinates [27].

Next, we describe three methods for polarizing a nuclear spin. In our simulations we consider a nucleus with spin $1/2$, i.e., ^{13}C or ^{15}N nuclear spin. However, the discussion is also valid for ^{14}N nuclear spin 1 . We label the basis states as $|m_s, m_I\rangle$, where the first component indicates the electron spin projection, $m_s = 0, \pm 1$, and the second component determines the nuclear spin projection \uparrow (\downarrow) corresponding to $m_I = \pm 1/2$, respectively.

A. Polarization at the level anti-crossing

One of the methods to polarize nuclear spins relies on the excited or ground state level anti-crossings, ESLAC and GSLAC respectively [4, 19]. Here, we focus on the ESLAC. In this approach, an external magnetic field, ≈ 510 G, is applied along the NV axis (z axis) so that the energy levels $m_s = -1$ and $m_s = 0$ in the excited state become very close (see Figure 3(a)). Under this configuration, the second term of the hyperfine Hamiltonian, Eq. (2), mixes states $|0, \downarrow\rangle$ and $|-1, \uparrow\rangle$ in the excited state. Note that $m_s = 1$ states ($|1, \downarrow\rangle$ and $|1, \uparrow\rangle$) are not mixed with $m_s = 0$ and $m_s = -1$ states because they are far away in energy.

This scheme polarizes the nuclear spin to $|\uparrow\rangle$, as we now explain [4]. At the ESLAC, the optical excitation transfers the electron from $|0, \downarrow\rangle$ ground state to $|0, \downarrow\rangle$ excited state. This is shown by red

arrows labeled by k in Fig. 3(a). In the excited state, the $A_{\perp}^{(e)}$ component of the hyperfine interaction causes precession between $|0, \downarrow\rangle$ and $|-1, \uparrow\rangle$ (shown by the blue arrow in Fig. 3(a)). During this precession the electronic spin may go to $|0, \uparrow\rangle$ in the ground state by passing through the metastable singlet state (shown by the red arrow labeled by γ). This polarization method relies primarily on the rates from the excited state to the singlet and secondarily on the rates from the singlet to the ground state.

Figure 3 shows the nuclear polarization for the ^{15}N nuclear spin at ESLAC. The hyperfine matrix for this nuclear spin is diagonal for both ground and excited states ($A_{\text{ani}} = 0$) and are given in Ref. [7]. In Fig. 3(a) we show the sequence for polarizing the nuclear spin. The dynamics of the nuclear and electronic polarizations are shown in Fig. 3(b). We indicate the electron polarization by the population in $m_s = 0$ state, while for the nuclear polarization we use

$$P_n = |\rho_n(\uparrow, \uparrow) - \rho_n(\downarrow, \downarrow)|, \quad (7)$$

where ρ_n is the reduced density matrix after tracing over the electronic spin.

We have calculated the density matrix evolution using the master equation [3, 27] assuming no initial polarization for both the electronic and nuclear spins. After few microseconds of optical excitation, the nuclear spin is polarized at a rate that is proportional to $A_{\perp}^{(e)}$. For more details see Refs. [4, 30]. In our simulations we have taken the transverse and longitudinal relaxation times of the NV electron spin as $T_{2,e}^* = 3 \mu\text{s}$ and $T_{1,e} = 1$ ms, respectively, and $T_{2,n}^* = 1$ ms and $T_{1,n} = 100$ ms for the nuclear spin. We have also neglected ionization effects of the NV center due to optical excitation [31].

As expected, once the optical excitation is turned off the optical excited and singlet populations relax to the ground state, increasing the electronic polarization. As the optical excitation rate increases, the nuclear polarization remains almost unchanged while the electronic polarization increases slightly for model 1 and decreases for the other models (see Fig. 3(c) and (d)). Figure 3(c) shows the nuclear polarization achieved for a specific electronic polarization where polarizations are parametrized by the optical excitation rate, k . The empty markers correspond to $k = 4$ MHz while the filled markers correspond to $k = 70$ MHz.

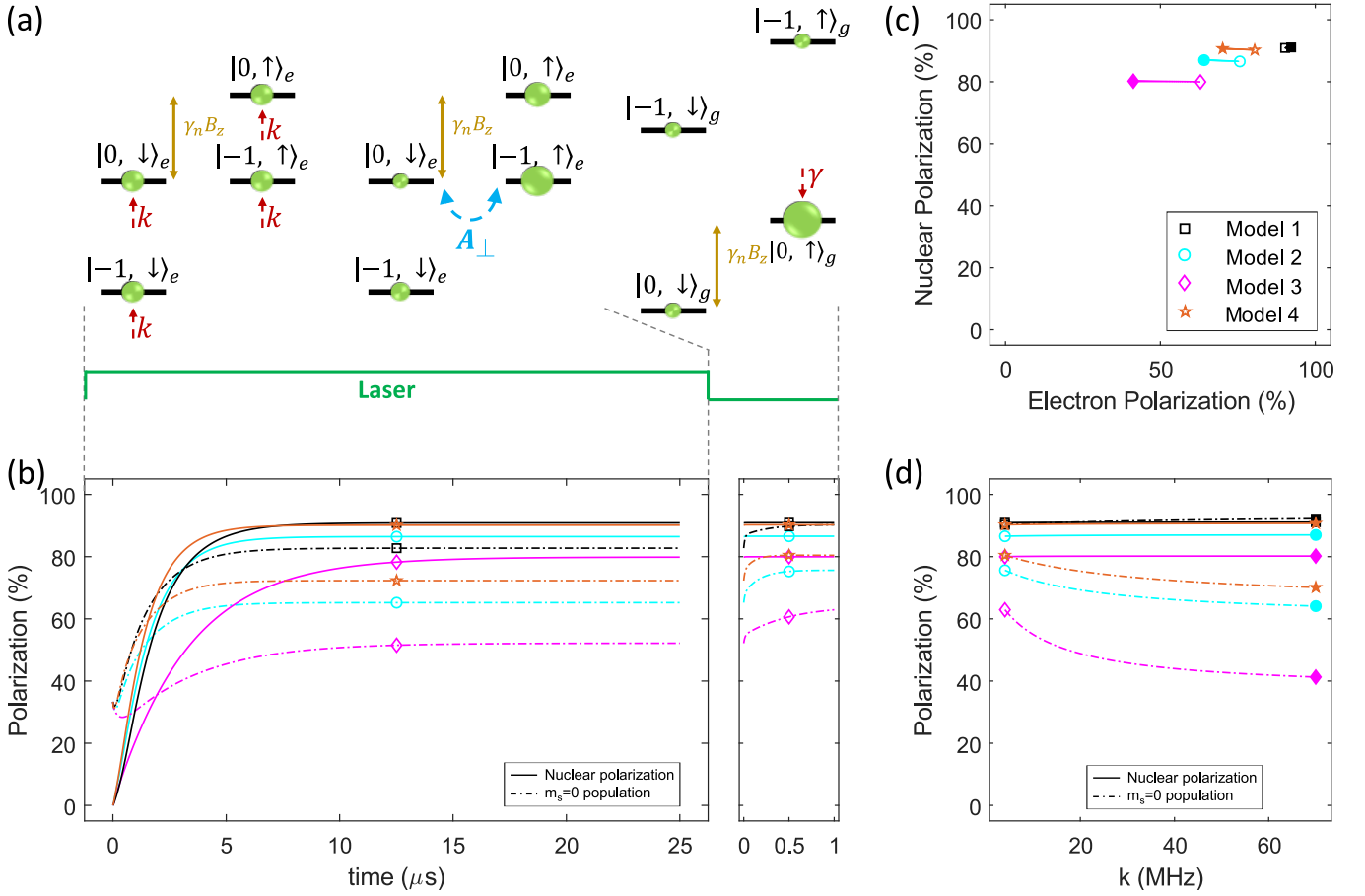


FIG. 3. Excited state level anti-crossing (ESLAC) nuclear spin polarization for the ^{15}N nuclear spin. (a) For a magnetic field of 512 G, the excited electronic spin states $m_s = 0$ and $m_s = -1$ become close in energy. The $A_{\perp}^{(e)}$ component of the hyperfine interaction causes flip-flops between $|0, \downarrow\rangle_e$ and $|-1, \uparrow\rangle_e$ states. As $m_s = -1$ excited state population decays to the $m_s = 0$ ground state, the nuclear spin is polarized to $|\uparrow\rangle$ state. The red dashed arrows, labeled by k and γ , represent the optical excitation to the excited state and the spontaneous decay to the ground state, respectively. (b) Electronic and nuclear spin polarization dynamics for $k = 4$ MHz for the four transition rate models given in Table I as in the legends of (c). Electron polarization increases at the end due to relaxation from the singlet. (c) Nuclear versus electronic spin polarizations parametrized as a function of the excitation rate k . The open markers correspond to $k = 4$ MHz, while the filled markers correspond to $k = 70$ MHz. (d) Electronic and nuclear polarization as a function of k .

Non-zero rates $k_{0,S}$ and $k_{S,\pm}$ contribute to the polarization of the opposite nuclear spin projection. In particular, a strong $k_{0,S}$ will result in increasing the population of $m_s = \pm 1$ on the ground state, which will contribute to rotate the nuclear spin from up to down. Indeed, model 3 has the smallest ratio between $k_{0,S}$ and $k_{\pm,S}$ and achieves the smallest nuclear polarization, whereas model 4 has the second largest ratio of these rates and achieves a high nuclear polarization together with model 1.

In the supplementary materials we show the nuclear spin polarization for ^{15}N as a function of the magnitude of the magnetic field along the NV axis for all the models [27]. We note that, for mag-

netic fields between ESLAC and GSLAC, the nuclear polarization achieved by our estimations, in the steady state, does not fit well with experiments of Ref. [4]. For this range of the magnetic fields, similar to Ref. [32], we achieve higher nuclear polarizations. Extra nuclear depolarization effects during optical excitation might explain this discrepancy.

We now discuss two other methods to optically polarize nuclear spins based on nuclear spin precession while the electron is in the electronic ground state.

B. Polarization by nuclear spin precession on $m_s = 0$

In this method, the electron spin is first optically pumped mostly to the $m_s = 0$ state, indicated by the red arrow labeled by γ in Fig. 4(a). After waiting for the population to decay to the ground state, a selective microwave pulse is applied in order to transfer the population from $|0, \downarrow\rangle$ to $|1, \downarrow\rangle$. Meanwhile, the nuclear spin precesses between $|0, \uparrow\rangle$ and $|0, \downarrow\rangle$, due to a perpendicular magnetic field (indicated by the blue arrow in Fig. 4(a)). Finally a laser pulse, followed by a waiting time, is used to leave the electron spin mostly in its $m_s = 0$ ground state (final red arrow labeled by γ in Fig. 4(a)).

This approach is a variation of the method proposed in Ref. [20]. In that work, a selective microwave π pulse is used, while here we find the optimal microwave time to achieve the maximum nuclear polarization [27]. This approach can be also understood by means of coherent population trapping (see Ref. [33] for details).

Figure 4(b) shows the dynamics of the electronic and nuclear polarization for a perpendicular magnetic field component of $B_x = 10$ G and a small parallel component of $B_z = 0.5$ G. The highest nuclear spin polarization is achieved after the microwave pulse and is proportional to the electron spin polarization achieved after the optical excitation and first waiting time. Figure 4(c) shows the electron and nuclear polarizations parametrized by the optical excitation rate, k . Similar to the ESLAC case, the empty markers correspond to $k = 4$ MHz and the filled markers correspond to $k = 70$ MHz. This method crucially depends on the electronic spin polarization. This dependence can be clearly observed by comparing the nuclear polarization at the end of the microwave with the electronic polarization at the end of the first waiting time, shown by the points on the dashed gray line. Models 2 and 3 show a smaller nuclear spin polarization as they have the smallest ratio between the rates $k_{S,0}$ and $k_{S,\pm}$, with model 3 having the smallest ratio. Model 1 shows higher nuclear polarization at larger optical excitations. However, models 2 to 4 show the opposite behavior.

The points that do not sit on the dashed gray line are polarizations at the end of the sequence, and show how the nuclear spin depolarizes under optical excitation [34]. We have chosen the time of

the second laser pulse, 300 ns, in such a way that we achieve polarization for both the electron and the nuclear spin at the end of the sequence. The second waiting time is chosen sufficiently large so that the nuclear spin can be recovered due to its precession, i.e., $\approx 1/(2|\Delta|)$ where Δ is the coupling between $|0, \uparrow\rangle$ and $|0, \downarrow\rangle$ states. It can be noted that during the second waiting time, the direction of the nuclear polarization changes for all models due to the precession of the nuclear spin about the external magnetic field B_x .

Figure 4(d) shows the nuclear and electronic polarizations as a function of the excitation rate k at the end of the sequence. Due to the short time of the second laser pulse, as the excitation rate increases, the electronic polarization increases for all the models. However, the nuclear polarization decreases because as the excitation rate increases, the depolarization of the nuclear spin increases. This observation together with experimental realization of the nuclear polarization as a function of the optical power can be used to test the validity of the transition rate models. Figure 4 is plotted for a carbon nuclear spin in family C. The classification of nuclear spins to families is proposed in Refs. [5, 6].

In our simulations for this method, we have used the secular approximation, i.e., we have only kept terms in the Hamiltonian (Eq. (S36)) proportional to S_z and have ignored the terms that contain S_x or S_y . We have taken the effect of the non-secular terms perturbatively by adding the following Hamiltonian [27, 37, 38]

$$H_{\text{soc}} = \frac{(3S_z^2 - 2)D + S_z\gamma_e B_z}{2(D^2 - \gamma_e^2 B_z^2)} \hat{M} + \frac{(2 - S_z^2)\gamma_e B_z - S_z D}{2(D^2 - \gamma_e^2 B_z^2)} \hat{N}, \quad (8)$$

where

$$\begin{aligned} \hat{M} = & 2\gamma_e [(A_{xx}B_x + A_{yx}B_y) I_x \\ & + (A_{xy}B_x + A_{yy}B_y) I_y \\ & + (A_{xz}B_x + A_{yz}B_y) I_z] \\ & + \gamma_e^2 B_{\perp}^2 \mathbf{1} + (\vec{A}_+ \cdot \vec{A}_-) \mathbf{1}, \end{aligned} \quad (9)$$

and

$$\hat{N} = i(\vec{A}_+ \times \vec{A}_-) \cdot \vec{I}. \quad (10)$$

Here, \vec{I} is a vector which its components are the nuclear spin matrices $\vec{I} = (I_x, I_y, I_z)$, and $\mathbf{1}$ is the 2×2 identity matrix.

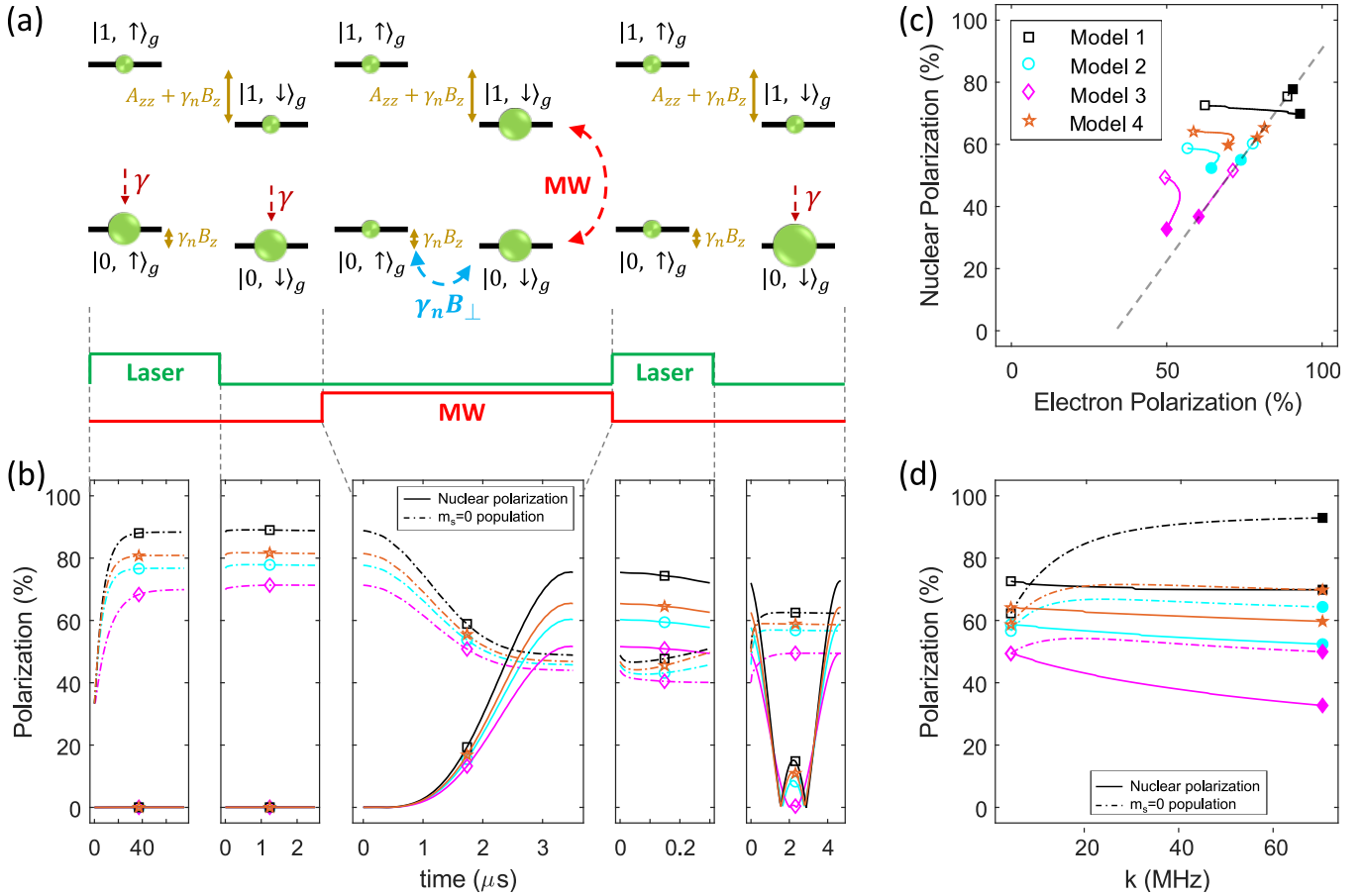


FIG. 4. Nuclear spin polarization by nuclear precession on electronic spin state $m_s = 0$. (a) After optical excitation and relaxation from the singlet, a selective microwave pulse transfers the $|0, \downarrow\rangle$ population to $|1, \downarrow\rangle$. At the same time a 10 G external magnetic field along the x axis, causes precession between $|0, \uparrow\rangle$ and $|0, \downarrow\rangle$. Finally, a second laser pulse transfers $|1, \downarrow\rangle$ to $|0, \downarrow\rangle$. The red dashed arrow γ , represents the spontaneous decay to the ground state. (b) Electronic and nuclear spin polarization dynamics for $k = 4$ MHz for the four transition rate models. After the electron spin is mostly polarized in $m_s = 0$ state, the electronic polarization is transferred to the nucleus by precession and microwave excitation. Finally, the electronic polarization is recovered by laser excitation. (c) Nuclear versus electronic spin polarization parametrized as a function of the optical excitation rate k . Open (filled) markers correspond to $k = 4$ MHz (70 MHz). The data on the dashed-gray line correspond to the electron spin polarization after the first waiting time and nuclear spin polarization after the MW. The data that does not sit on the dashed-gray line correspond to the polarizations at the end of the sequence. (d) Electronic and nuclear polarization at the end of the sequence as a function of k . This figure is plotted for a ^{13}C nuclear spin in family C.

Note that, $|\uparrow\rangle$ and $|\downarrow\rangle$ are the eigenstates when the electronic spin is in $m_s = 1$ of the ground state. For $m_s = 0$ electron spin, the hyperfine Hamiltonian is zero and the off-axis magnetic field (shown by the blue arrow in Fig. 4(a)) together with the correction given in Eq. (8) determine the quantization axis of the nuclear spin. The precession rate is given by $\gamma_n B (1 - |\hat{n}_{m_s=0} \cdot \hat{n}_{m_s=1}|)$ where $\hat{n}_{m_s=0}$ is the unit vector that indicates the quantization axis of the nuclear spin while the electron is in the $m_s = 0$ which is mostly determined by the external magnetic field. On the other hand, $\hat{n}_{m_s=1}$ is

the unit vector in the direction of the quantization axis of the nuclear spin while the electron is in the $m_s = 1$ state, i.e., in the direction mostly determined by $\mathbf{A}_z + \gamma_n \mathbf{B}$. Therefore, there is an optimal perpendicular magnetic field that results in a higher polarization at the end of the sequence. If the magnetic field is too low, it results in a lower polarization after the microwave. While if the magnetic field is too high, both quantization axes are similar and the precession does not take place either.

We finish this section by noting that the nuclear polarization can be improved by repeatedly apply-

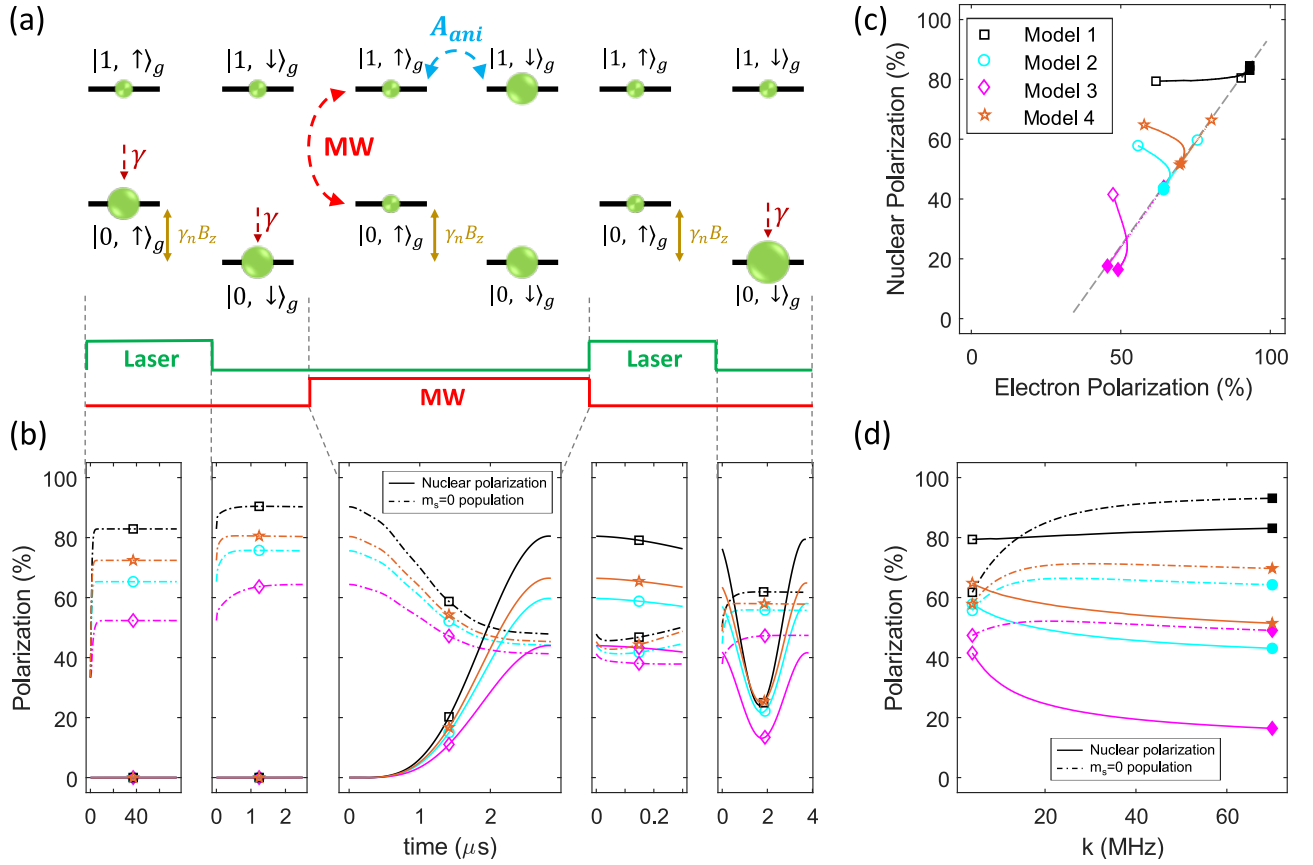


FIG. 5. Nuclear spin polarization by nuclear precession on electronic spin state $m_s = 1$. (a) The electronic spin is polarized to $m_s = 0$ state by an optical pulse followed by a waiting time. A selective microwave pulse is then applied to transfer the population from $|0, \uparrow\rangle$ to $|1, \uparrow\rangle$. At the same time, the anisotropic component of the hyperfine interaction causes precession between $|1, \uparrow\rangle$ and $|1, \downarrow\rangle$. Finally, a second laser pulse is used to transfer the $|1, \downarrow\rangle$ to $|0, \downarrow\rangle$. The external magnetic field is aligned to the NV axis. The red dashed arrow, γ , represents the spontaneous decay to the ground state. (b) Electronic and nuclear spin polarization dynamics for $k = 4$ MHz for the four transition rate models. After electronic population is relaxed from the singlet, the electronic polarization is transferred to the nuclear polarization by precession and microwave excitation. Finally, the electronic polarization is recovered by laser excitation keeping the nuclear polarization. (c) Nuclear spin polarization versus electronic spin polarization parametrized as a function of the optical excitation rate k . The open (filled) markers correspond to the optical excitation rate $k = 4$ MHz (70 MHz). The data on the gray dashed line correspond to the electron spin polarization after the first waiting time and nuclear spin polarization after the MW. The data that does not sit on the dashed-gray line corresponds to the polarizations at the end of the sequence. (d) Electronic and nuclear polarization at the end of the sequence as a function of k . In this figure we have considered a ^{13}C nuclear spin in family H.

ing the sequence on Fig. 4(a) [20].

C. Polarization by nuclear spin precession on $m_s = 1$

Finally, it is possible to achieve nuclear polarization while the electronic spin is in the $m_s = 1$ state [21]. In this case, it makes sense to consider a nuclear spin basis given by the nuclear spin eigenstates while the electronic spin is in the $m_s = 0$ state. We take the magnetic field to be aligned with the NV

axis for which a higher electronic spin polarization is achieved. The precession relies on the anisotropic component of the hyperfine interaction, which depends on the relative orientation of the nuclear spin with respect to the NV axis, as it can be seen from Eq. (5).

For the precession in $m_s = 1$ state to occur, we apply a magnetic field along the NV axis that brings the ground states $|1, \uparrow\rangle$ and $|1, \downarrow\rangle$ very close, i.e., $B_z = -A_{zz}/\gamma_n$. For nearby nuclear spins, which have A_{zz} of the order of few MHz, this method requires very large magnetic fields, of the order of few

thousand Gauss. Therefore, this method may be experimentally more accessible for far ^{13}C nuclear spins which have A_{zz} of the order of few hundred kHz, family J and families further away. For polarizing such nuclear spins, with this method, magnetic fields below 1000 G are required (see Fig. 6(f)).

Figure 5(a) illustrates a typical configuration of this protocol. First the electron is optically polarized to the ground $m_s = 0$ state (indicated by the red arrow labeled by γ in Fig. 5(a)) followed by a waiting time. Then a selective microwave excitation transfers the population from $|0, \uparrow\rangle$ to $|1, \uparrow\rangle$. Due to the anisotropic component of the hyperfine interaction, the nuclear spin precesses between the states $|1, \uparrow\rangle$ and $|1, \downarrow\rangle$. This process effectively transfers the electronic polarization to the nuclear spin polarization.

It is clear that if the electronic polarization is not perfect, neither is the nuclear polarization. This effect can be seen in Fig. 5(c) where both polarizations are plotted parametrized by the excitation rate. Similar to the method based on precession in the $m_s = 0$ state, data points on the dashed gray line correspond to the electronic polarization after the first waiting time and the nuclear polarization after the microwave. The data points that sit outside the dashed line correspond to the polarizations after the second waiting time. Here, we have chosen the time of the second laser pulse and the second waiting time similar to the method based on precession on $m_s = 0$ state.

The discussion for figures 4(c) and (d) is also relevant here except for the nuclear polarization for model 1 at the end of the sequence. For that model, as the excitation rate increases the nuclear polarization increases. The difference relies on the precession of the nuclear spin. For the polarization based on precession while the electron is in the $m_s = 0$ state, the nuclear spin precesses along the external magnetic field at all times. However, for the polarization based on precession while the electron is on the $m_s = 1$ state, the nuclear spin precesses only when the electron is on the $m_s = 1$ state. As shown in Figures 5(c) and (d), models 2-4 that predict smaller electronic polarization also show smaller nuclear polarization, especially at large optical powers. Figure 5 is plotted for a ^{13}C nuclear spin in family H.

In the following Section we discuss the dependence of electronic and nuclear spin polarizations

on the optical power and the transition rate model.

IV. DISCUSSION

We now analyze in detail the nuclear polarization dependence on the transition rates involved in the inter-system crossing and on the angular position of the nuclear spin relative to the NV axis.

A. Power dependence of electronic and nuclear polarization

As mentioned earlier in Section II, the electronic spin polarization crucially depends on the transition rates and the optical power, which in turn, might affect the polarization of nearby nuclear spins. The nuclear spin polarization method based on the ES-LAC is the one less affected by this phenomenon. For this method, the nuclear polarization depends mainly on the transfer of electronic spin population from the excited state to the singlet. As $m_s = \pm 1$ population is transferred the most to the singlet, the nuclear spin $|\uparrow\rangle$ prevails. However, a finite nuclear spin polarization is caused by non-zero rates $k_{0,S}$ and $k_{S,\pm}$ which contribute to polarize the nuclear spin in the opposite state. As these rates are zero for model 1, a high nuclear polarization for ^{15}N nuclear spin, ≈ 0.9 , close to the experimental value 0.96 [4], is achieved for model 1. However, this model allows for non-spin preserving transitions modeled by e . A smaller value for e results in a higher nuclear polarization. Model 4 achieves the second highest polarization as it has the largest ratio between the rates $k_{\pm,S}$ and $k_{0,S}$. Moreover, model 4 has zero non-spin preserving transition, i.e., $e = 0$. When $m_s = \pm 1$ is partially populated, A_{\perp} component of the hyperfine interaction causes opposite nuclear spin transition from $|\downarrow\rangle$ to $|\uparrow\rangle$ resulting in a lower nuclear spin polarization.

The nuclear polarization methods based on precession described in Sections IIIB and IIIC are readily affected by a finite electronic spin polarization. They rely on the transfer of polarization from the electronic to the nuclear spin. Therefore, the polarization of the nuclear spin cannot be larger than the electronic polarization as it can be appreciated in Figs. 4(c) and 5(c) (points on the gray dashed line). For model 1, the higher the power of the first laser pulse, the higher the nuclear polarization.

However, for the other models, the higher the optical power, the lower the electronic polarization. As a result, a lower nuclear polarization is achieved after the microwave. The second laser pulse, used to polarize the electronic spin, results in depolarization of the nuclear spin [34]. Figures 4(c) and 5(c) show that the higher the optical power of the second laser pulse, the lower the nuclear polarization achieved at the end of the sequence.

Further measurements are needed to determine which of these transition rate models is more accurate. For instance, the degree of nuclear spin polarization can be observed by analyzing the Fourier transform of Ramsey experiments. These measurements together with the previous discussion can be used to validate a transition rate model or even to measure these rates more accurately. In addition, the dependence on the optical power is also important and it must be taken into account if a large nuclear spin polarization is meant to be achieved.

B. Anisotropy dependence of nuclear spin polarization

Each of the nuclear polarization methods relies on different components of the hyperfine interaction, which in turn depends on the angular position of the nuclear spin relative to the NV axis. In this section we discuss the polarization performance as a function of the polar distribution of the nuclear spins relative to the NV axis. Moreover, we estimate the nuclear spin polarization for a range of families.

The method based on ESLAC takes advantage of the perpendicular component of the hyperfine interaction, A_{\perp} , to cause flip-flops between the electron and nuclear spins. If $A_c > A_d$, A_{\perp} is nonzero for all angles θ_H . For $A_c \leq A_d$, there are two angles for which $A_{\perp} = 0$. For zero contact term ($A_c = 0$), we have $A_{\perp} = 0$ if $\theta_H = \pm \arccos(1/\sqrt{3}) \approx \pm 54$ deg. For far nuclear spins A_{\perp} decreases, and as a result, the nuclear polarization rate decreases, requiring longer times to achieve polarization. On the other hand, the final polarization decreases as the A'_{\perp} and A_{ani} components of the hyperfine interaction increases [27]. Therefore, the achieved nuclear polarization depends on the polar angle θ_H (Fig. 6(a)).

Figure 6(b) shows the polarization for ^{15}N and families A to H, whose hyperfine matrices are taken from Ref. [7]. The polarization is smaller for families

that have A_{ani} and A'_{\perp} components comparable to A_{\perp} . In the supplementary materials we compare our simulated polarization for those families with the experimental data of Refs. [4–6].

The methods based on nuclear precession while the electronic spin is in $m_s = 0$, and $m_s = 1$ depend on an external magnetic field perpendicular to the nuclear quantization axis $\mathbf{\Omega}_1 = \mathbf{A}_z + \gamma_n \mathbf{B}$, where $\mathbf{A}_z = (A_{\text{ani}} \cos \varphi_H, A_{\text{ani}} \sin \varphi_H, A_{zz})$. In other words, defining $\mathbf{\Omega}_0 = \gamma_n \mathbf{B}$, the magnetic field should be chosen such that

$$\mathbf{\Omega}_1 \cdot \mathbf{\Omega}_0 = 0. \quad (11)$$

As we have taken the azimuthal angle of the nuclear spin to be $\varphi_H = 0$ [27], a magnetic field that satisfies Eq. (11) is given by $\mathbf{B} = B\hat{x} = -(A_{\text{ani}}/\gamma_n)\hat{x}$. This perpendicular magnetic field could be very large for nuclear spins with A_{ani} of the order of few hundred kHz. As this magnetic field is present during the whole sequence, we choose it smaller than 50 G in order to achieve a high electronic polarization in the method based on precession on $m_s = 0$. In addition, the magnetic field should be taken such that it does not change the quantization axis of the nuclear spin, i.e., $B \ll |\mathbf{A}_z|/\gamma_n$.

Fig. 6(c) shows a small dependence on θ_H because the correction term for the Hamiltonian (Eq. (8)) depends on non-diagonal elements of the hyperfine matrix, which in turn depend on θ_H . In fact, a relatively lower polarization is achieved for family H, for which this correction reduces the nuclear spin precession (Fig. 6(d)).

For the polarization method based on precession on $m_s = 1$, the magnetic field is taken along the z axis ($\mathbf{\Omega}_0 = \Omega_0\hat{z}$), and following Eq. (11), is given by $B = -A_{zz}/\gamma_n$. Having the magnetic field along the NV axis, results in a higher electron spin polarization as non-spin-preserving transitions are minimized. For this method, the precession between the nuclear spin states occurs due to the anisotropic component of the hyperfine interaction A_{ani} , which is zero at $\theta_H = \{0, \pi/2, \pi\}$ (see Fig. 1). At these angles, no precession takes place and no nuclear spin polarization is achieved (see Fig. 6(e)).

Figure 6(f) shows the nuclear polarization for families H to O2. We have taken the hyperfine matrix for families I to O2 from Ref. [39]. In that work, the hyperfine matrix is only given for the ground state of the NV center. As an approximation, we

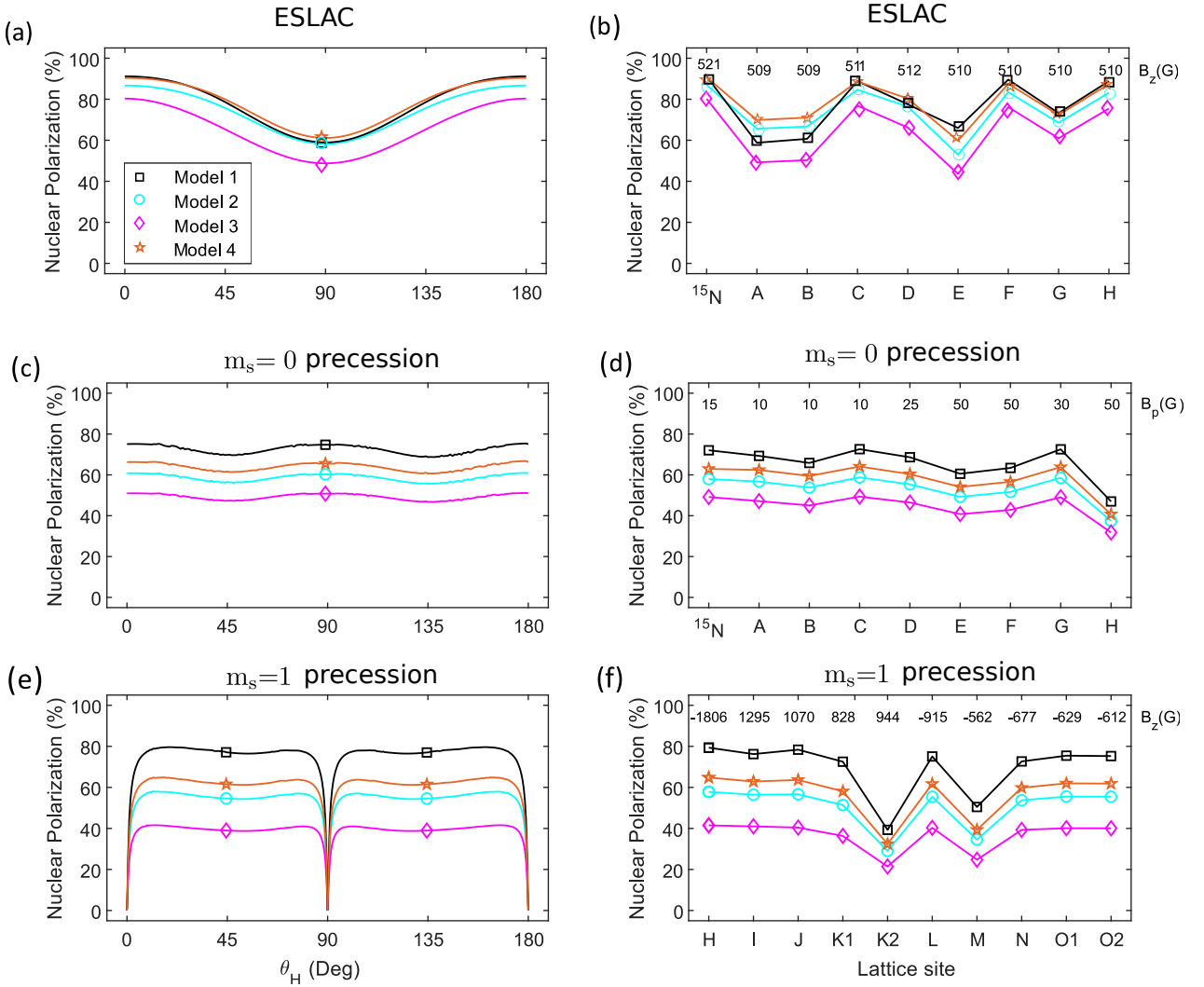


FIG. 6. Nuclear polarization versus θ_H for the method based on ESLAC (a), precession in $m_s = 0$ (c), and precession in $m_s = 1$ (e). In these plots we have respectively used the contact and dipole terms corresponding to families C, C, and H, setting $\varphi_H = 0$. In (b), (d) and (f) we show the nuclear polarization achieved with different methods for a range of families. In these figures, the upper horizontal axes show the magnetic field for each family.

have used the same hyperfine matrix for the excited state. A lower polarization is achieved for families K2 and M. Family K2 has a small anisotropic term resulting in a low nuclear polarization. For family M, A_{ani} is large enough that can cause transitions between $|0, \downarrow(\uparrow)\rangle$ and $|1, \downarrow(\uparrow)\rangle$, therefore, reducing the nuclear polarization. This method of polarization cannot be used to polarize the ^{15}N as the hyperfine matrix of the nitrogen nuclear spin is diagonal and the anisotropic term is zero.

As a summary, for nuclear spins close to the NV center, polarization can be achieved using methods based on ESLAC and precession of electron spin while being on $m_s = 0$ state. For such nuclear spins the method based on precession in $m_s = 1$

requires very large magnetic fields and therefore is more susceptible to magnetic field misalignments. For far nuclear spins the methods based on $m_s = 0$ and $m_s = 1$ precession could be used. The ESLAC method for far nuclear spins requires a very long laser time and it will be limited by non-spin-preserving transitions.

V. CONCLUSIONS

We have shown that the electronic spin polarization crucially depends on the transition rates involved in the inter system crossing, which indirectly affects the nuclear spin polarization. We considered four models for these rates based on previous ex-

periments [13–16] and analyzed the effects on the electronic and nuclear polarization for three polarization methods.

For model 1 [13], the electronic polarization increase with the optical power, while for model 2 [14], 3 [15], and 4 [16] the electronic polarization decreases with optical power. This is caused by non-spin preserving transition rates and non zero transition rates from the excited $m_s = 0$ state to the singlet and from the singlet to the $m_s = \pm 1$ ground states.

The nuclear polarization method which is less affected by the optical power is that based on the ESLAC for which the nuclear polarization changes very slightly for all the transition rate models. Still this method is affected by the new proposed non-radiative rates of several recent experimental works. As discussed, some of them lead to too small nuclear polarization, contrary to experimental observations.

The other two methods that rely on nuclear spin precession on the ground state (either $m_s = 0$ or $m_s = 1$) are greatly affected by a finite electronic spin polarization. This is because during the precession, at most, the electron spin polarization is

transferred to the nuclear spin polarization. We have also compared the polarization performance of three methods depending on the angular position of the nuclear spin relative to the NV axis.

This analysis together with measurements that involve the nuclear spin polarization can be used to determine the transition rates of the inter-system crossing and give directions to achieve larger nuclear spin polarizations. Enhancing the polarization of nuclear spins could result in the enhancement of the NMR and magnetic resonance imaging. Moreover, it could enhance the coherence time of the NV electron spin.

ACKNOWLEDGMENTS

The authors thank A. Dréau for helpful discussions. H.D. acknowledges support from Conicyt doctorado grant No. 21100070. H.T.D. acknowledges support from the Fondecyt-postdoctorado grant No. 3170922. J.R.M. acknowledges support from Fondecyt Regular Grant No. 1180673, Air Force grant number FA9550-18-1-0513, and Anid-PIA ACT192023. H.T.D., V.J. and J.R.M. acknowledge support from Conicyt-ECOS grant C16E04.

-
- [1] G. D. Fuchs, G. Burkard, P. V. Klimov, and D. D. Awschalom, *Nat. Phys.* **7**, 789 (2011).
 - [2] P. C. Maurer, G. Kucsko, C. Latta, L. Jiang, N. Y. Yao, S. D. Bennett, F. Pastawski, D. Hunger, N. Chisholm, M. Markham, D. J. Twitchen, J. I. Cirac, M. D. Lukin, *Science* **336**, 1283 (2012).
 - [3] P. Neumann, J. Beck, M. Steiner, F. Rempp, H. Fedder, P. Hemmer, J. Wrachtrup, and F. Jelezko, *Science* **329**, 542 (2010).
 - [4] R. Coto, H. T. Dinani, A. Norambuena, M. Chen, J. R. Maze, arXiv:2003.11925v2 (2020).
 - [5] J. R. Maze, P. L. Stanwix, J. S. Hodges, S. Hong, J. M. Taylor, P. Cappellaro, L. Jiang, M. V. G. Dutt, E. Togan, A. S. Zibrov, A. Yacoby, R. L. Walsworth, and M. D. Lukin, *Nature (London)* **455**, 644 (2008).
 - [6] L. Rondin, J-P. Tetienne, T. Hingant, J-F. Roch, P. Maletinsky, and V. Jacques, *Rep. Prog. Phys.* **77** 056503 (2014).
 - [7] C. Bonato, M. S. Blok, H. T. Dinani, D.W. Berry, L. Markham, D. J. Twichen, and R. Hanson, *Nat. Nanotechnol.* **11**, 247 (2016).
 - [8] H. T. Dinani, D. W. Berry, R. Gonzalez, J. R. Maze, and C. Bonato, *Phys. Rev. B* **99**, 125413 (2019).
 - [9] J. Wrachtrup, F. Jelezko, *J. Phys.: Condens. Matter* **18** S807 (2006).
 - [10] G. Balasubramanian, P. Neumann, D. Twitchen, M. Markham, R. Kolesov, N. Mizuochi, J. Isoya, J. Achard, J. Beck, J. Tessler, V. Jacques, P. R. Hemmer, F. Jelezko, and J. Wrachtrup, *Nat. Mater.* **8** 383 (2009).
 - [11] Y. Chu, M. Markham, D. J. Twitchen, and M. D. Lukin, *Phys. Rev. A* **91**, 021801(R) (2015).
 - [12] M. W. Doherty, N. B. Manson, P. Delaney, F. Jelezko, J. Wrachtrup, L. C. L. Hollenberg, *Phys. Rep.* **528**, 1 (2013).
 - [13] N. Manson, J. Harrison, and M. Sellars, *Phys. Rev. B* **74**, 104303 (2006).
 - [14] L. Robledo, H. Bernien, T. Van Der Sar, and R. Hanson, *New J. Phys.* **13**, 025013 (2011).
 - [15] J. Tetienne, L. Rondin, P. Spinicelli, M. Chipaux, T. Debuisschert, J. Roch, and V. Jacques, *New J. Phys.* **14**, 103033 (2012).
 - [16] A. Gupta, L. Hacquebard, and L. Childress, *J. Opt. Soc. Am. B* **33**, B28 (2016).
 - [17] L. Hacquebard, and L. Childress, *Phys. Rev. A* **97**, 063408 (2018).
 - [18] V. Jacques, P. Neumann, J. Beck, M. Markham, D. Twitchen, J. Meijer, F. Kaiser, G. Balasubramanian, F. Jelezko, and J. Wrachtrup, *Phys. Rev. Lett.* **102**, 057403 (2009).

- [19] H-J. Wang, C. S. Shin, C. E. Avalos, S. J. Seltzer, D. Budker, A. Pines, and V. S. Bajaj, *Nat. Comm.* **4**, 1940 (2013).
- [20] M. V. G. Dutt, L. Childress, L. Jiang, E. Togan, J. Maze, F. Jelezko, A. S. Zibrov, P. R. Hemmer, and M. D. Lukin, *Science* **316**, 1312 (2007).
- [21] M. P. Jamonneau, PhD thesis, L'Université Paris-Saclay (2016).
- [22] J. Yun, K. Kim, D. Kim, *New J. Phys.* **21**, 093065 (2019).
- [23] J. Zhang, S. Hegde, D. Suter, *Phys. Rev. Applied* **12**, 064047 (2019).
- [24] P. Neumann, R. Kolesov, V. Jacques, J. Beck, J. Tisler, A. Batalov, L. Rogers, N. B. Manson, G. Balasubramanian, F. Jelezko, and J. Wrachtrup, *New J. Phys.* **11**, 013017 (2009).
- [25] A. Gali, M. Fyta, and E. Kaxiras, *Phys. Rev. B* **77**, 155206 (2008).
- [26] A. P. Nizovtsev, S. Ya Kilin, A. L. Pushkarchuk, V. A. Pushkarchuk, S. A. Kuten, O. A. Zhikol, S. Schmitt, T. Uden, and F. Jelezko, *New J. Phys.* **20**, 023022 (2018).
- [27] See Supplementary Materials for details.
- [28] V. Ivády, K. Szász, A. L. Falk, P. V. Klimov, D. J. Christle, E. Janzén, I. A. Abrikosov, D. D. Awschalom, and A. Gali, *Phys. Rev. B* **92**, 115206 (2015).
- [29] T. Havel, *J. Math. Phys.* **44**, 534 (2003).
- [30] A. Gali, *Phys. Rev. B* **80**, 241204(R) (2009).
- [31] F. Poggiali, P. Cappellaro, and N. Fabbri, *Phys. Rev. B* **95**, 195308 (2017).
- [32] S. Nah, *Mater. Res. Express* **3**, 075008 (2016).
- [33] L. Nicolas, T. Delord, P. Jamonneau, R. Coto, J. R. Maze, V. Jacques, and G. Hétet, *New J. Phys.* **20**, 033007 (2018).
- [34] L. Jiang, M. V. Gurudev Dutt, E. Togan, L. Childress, P. Cappellaro, J. M. Taylor, and M. D. Lukin, *Phys. Rev. Lett.* **100**, 073001 (2008).
- [35] A. Dréau, J. R. Maze, M. Lesik, J. F. Roch, and V. Jacques, *Phys. Rev. B* **85**, 134107 (2012).
- [36] B. Smeltzer, L. Childress, A. Gali, *New J. Phys.* **13**, 025021 (2011).
- [37] J. R. Maze, J. M. Taylor, and M. D. Lukin, *Phys. Rev. B* **78**, 094303 (2008).
- [38] L. Childress, M. V. G. Dutt, J. M. Taylor, A. S. Zibrov, F. Jelezko, J. Wrachtrup, P. R. Hemmer, and M. D. Lukin, *Science* **314**, 281 (2006).
- [39] A. P. Nizovtsev, S. Ya Kilin, A. L. Pushkarchuk, V. A. Pushkarchuk, and F. Jelezko, *New J. Phys.* **16**, 083014 (2014).

Supplemental Materials: Effect of inter-system crossing rates and optical illumination on the polarization of nuclear spins nearby nitrogen-vacancy centers

HYPERFINE INTERACTION HAMILTONIAN

In this section we show how the hyperfine Hamiltonian can be written as given in Eq. (2) of the main text. The hyperfine part of the Hamiltonian in tensor form is given as $\mathbf{S} \cdot \mathbf{A} \cdot \mathbf{I}$ which can be written as

$$\begin{aligned} \mathbf{S} \cdot \mathbf{A} \cdot \mathbf{I} = & S_x I_x A_{xx} + S_x I_y A_{xy} + S_x I_z A_{xz} \\ & + S_y I_x A_{yx} + S_y I_y A_{yy} + S_y I_z A_{yz} \\ & + S_z I_x A_{zx} + S_z I_y A_{zy} + S_z I_z A_{zz}. \end{aligned} \quad (\text{S1})$$

Writing x and y components of the electron and nuclear spin operators in terms of spin ladder operators, i.e.,

$$S_x = \frac{1}{2}(S_+ + S_-), \quad S_y = \frac{-i}{2}(S_+ - S_-), \quad (\text{S2})$$

$$I_x = \frac{1}{2}(I_+ + I_-), \quad I_y = \frac{-i}{2}(I_+ - I_-), \quad (\text{S3})$$

we can write

$$\begin{aligned} 4\mathbf{S} \cdot \mathbf{A} \cdot \mathbf{I} = & (S_+ + S_-)(I_+ + I_-)A_{xx} - i(S_+ + S_-)(I_+ - I_-)A_{xy} \\ & - i(S_+ - S_-)(I_+ + I_-)A_{yx} - (S_+ - S_-)(I_+ - I_-)A_{yy} \\ & + 2(S_+ + S_-)I_z A_{xz} - 2i(S_+ - S_-)I_z A_{yz} \\ & + 2S_z(I_+ + I_-)A_{zx} - 2iS_z(I_+ - I_-)A_{zy} + 4S_z I_z A_{zz}. \end{aligned} \quad (\text{S4})$$

After some straightforward calculations and taking into account that $A_{ij} = A_{ji}$, for $i \neq j$, with i and j being x, y, z , we obtain

$$\begin{aligned}
4\mathbf{S} \cdot \mathbf{A} \cdot \mathbf{I} = & 4S_z I_z A_{zz} \\
& +(A_{xx} + A_{yy})(S_+ I_- + S_- I_+) \\
& + S_+ I_+ (A_{xx} - A_{yy} - 2iA_{xy}) \\
& + S_- I_- (A_{xx} - A_{yy} + 2iA_{xy}) \\
& + 2(S_+ I_z + S_z I_+) (A_{xz} - iA_{yz}) \\
& + 2(S_- I_z + S_z I_-) (A_{zx} + iA_{zy}).
\end{aligned} \tag{S5}$$

The components of the hyperfine matrix are given as [S1]

$$A_{xx} = A_c - A_d (1 - 3 \sin^2 \theta \cos^2 \varphi), \tag{S6}$$

$$A_{yy} = A_c - A_d (1 - 3 \sin^2 \theta \sin^2 \varphi), \tag{S7}$$

$$A_{zz} = A_c - A_d (1 - 3 \cos^2 \theta), \tag{S8}$$

$$A_{xy} = A_{yx} = 3A_d \sin^2 \theta \cos \varphi \sin \varphi, \tag{S9}$$

$$A_{xz} = A_{zx} = 3A_d \sin \theta \cos \theta \cos \varphi, \tag{S10}$$

$$A_{yz} = A_{zy} = 3A_d \sin \theta \cos \theta \sin \varphi, \tag{S11}$$

where θ and φ are the polar and azimuthal angles that determine the nuclear spin, shown in Fig. 1 of the main text. Here, to keep the notation simple we have removed the index H of the angles. Therefore we can write

$$A_{xx} - A_{yy} \pm 2iA_{xy} = 3A_d \sin^2 \theta e^{\pm i2\varphi}, \tag{S12}$$

$$A_{xz} \pm iA_{zy} = 3A_d \cos \theta \sin \theta e^{\pm i\varphi}. \tag{S13}$$

The hyperfine term can then be written as

$$\begin{aligned}
4\mathbf{S} \cdot \mathbf{A} \cdot \mathbf{I} = & 4S_z I_z A_{zz} \\
& +(2A_c - A_d(2 - 3 \sin^2 \theta))(S_+ I_- + S_- I_+) \\
& + 3A_d \sin^2 \theta (S_+ I_+ e^{-2i\varphi} + S_- I_- e^{+2i\varphi}) \\
& + 6A_d \cos \theta \sin \theta ((S_+ I_z + S_z I_+) e^{-i\varphi} + (S_- I_z + S_z I_-) e^{+i\varphi}).
\end{aligned} \tag{S14}$$

Defining

$$A_{\perp} = 2A_c + A_d (1 - 3 \cos^2 \theta), \tag{S15}$$

$$A_{ani} = 3A_d \cos \theta \sin \theta, \tag{S16}$$

$$A'_{\perp} = 3A_d \sin^2 \theta, \tag{S17}$$

we obtain

$$\begin{aligned}
\mathbf{S} \cdot \mathbf{A} \cdot \mathbf{I} = & S_z I_z A_{zz} \\
& + \frac{A_{\perp}}{4} (S_+ I_- + S_- I_+) \\
& + \frac{A'_{\perp}}{4} (S_+ I_+ e^{-2i\varphi} + S_- I_- e^{+2i\varphi}) \\
& + \frac{A_{ani}}{2} ((S_+ I_z + S_z I_+) e^{-i\varphi} + (S_- I_z + S_z I_-) e^{+i\varphi}).
\end{aligned} \tag{S18}$$

SUPEROPERATOR MASTER EQUATION

To find out the evolution of the density matrix of the combined system of an electron and nuclear spin we use the Markovian master equation [S2]

$$\frac{d\rho}{dt} = -i[H, \rho] + \sum_k \mathcal{D}(L_k)\rho, \quad (\text{S19})$$

in which

$$\mathcal{D}(L_k)\rho = L_k\rho L_k^\dagger - \frac{1}{2}\{\rho, L_k^\dagger L_k\}. \quad (\text{S20})$$

The first term in the master equation is the unitary evolution of the density matrix due to the total Hamiltonian of the system, while the second term is the evolution due to the interaction with the environment and is called Lindbladian. The operators L_k are known as the jump operators and cause transition between states of the system due to the interaction with the environment.

In our simulations we included the transitions between the states, due to the optical excitation and decay, through the Lindbladian part. For instance, the jump operator that represents the transition from the electron spin state $|i\rangle$ to $|j\rangle$ is given by $\sqrt{\alpha_{ij}}|i\rangle\langle j| \otimes \mathbf{1}$. Here, α_{ij} is the transition rate from the electron spin state $|i\rangle$ to $|j\rangle$ and $\mathbf{1}$ is the nuclear spin identity matrix. The effect of the inhomogeneous decoherence time, T_2^* , can be explained by a jump operator of the form $\frac{1}{\sqrt{2T_2^*}}S_z \otimes \mathbf{1}$.

In our simulations we used the vectorized form of the master equation given as [S3]

$$\frac{d\hat{\rho}(t)}{dt} = \mathcal{L}\hat{\rho}(t), \quad (\text{S21})$$

in which

$$\mathcal{L} = i(\bar{H} \otimes I - I \otimes H) + \sum_k \left(\bar{L}_k \otimes L_k - \frac{1}{2}I \otimes L_k^\dagger L_k - \frac{1}{2}\bar{L}_k^\dagger \bar{L}_k \otimes I \right). \quad (\text{S22})$$

Here, I is the $N \times N$ identity matrix where $N = 14$ is the dimension of the system of the NV electron and a spin 1/2 nuclear spin. The complex conjugate is shown with over bar and adjoint with dagger. The vector form of the density matrix, $\hat{\rho}$, is obtained by stacking the columns of the density matrix from left to right on top of each other. The time evolved density matrix is therefore obtained by

$$\hat{\rho}(t) = e^{\mathcal{L}t}\hat{\rho}(0). \quad (\text{S23})$$

RABI FREQUENCY AND OPTIMAL MICROWAVE TIME

In the methods based on the precession of nuclear spin while the electron spin is in $m_s = 0$ and while in $m_s = 1$, the electronic spin is under a microwave excitation while the nuclear spin is under an external magnetic field ($m_s = 0$) or the hyperfine interaction ($m_s = 1$). In order to find an analytical formula for the optimal Rabi frequency and the optimal time for the microwave field, we approximate the Hamiltonian of the electron-nuclear spin with a system of three levels. We consider the three levels which are close to each other energetically. In other words, for the $m_s = 0$ method we only consider $|0, \downarrow\rangle$, $|0, \uparrow\rangle$, and $|1, \downarrow\rangle$ and for the $m_s = 1$ method $|1, \downarrow\rangle$, $|1, \uparrow\rangle$, and $|0, \uparrow\rangle$ states.

With this approximation, in the microwave rotating frame, the Hamiltonian can be written as

$$H = \begin{pmatrix} 0 & \Delta & \Omega \\ \Delta & 0 & 0 \\ \Omega & 0 & 0 \end{pmatrix}. \quad (\text{S24})$$

Here, Δ is the nuclear coupling and Ω is the electronic coupling. We have also approximated all the diagonal terms with a same value which we have set to zero. This can be achieved through the proper choice of the magnetic field and microwave power. The eigenvalues of this Hamiltonian are

$$\lambda_0 = 0, \quad (\text{S25})$$

$$\lambda_{\pm} = \pm\sqrt{\Delta^2 + \Omega^2} = \pm\lambda, \quad (\text{S26})$$

and its eigenvectors are

$$v_0 = \frac{1}{\sqrt{\Delta^2 + \Omega^2}} \begin{bmatrix} 0, & \Omega, & -\Delta \end{bmatrix}, \quad (\text{S27})$$

$$v_{\pm} = \frac{1}{\sqrt{2(\Delta^2 + \Omega^2)}} \begin{bmatrix} \sqrt{\Delta^2 + \Omega^2}, & \pm\Delta, & \pm\Omega \end{bmatrix}. \quad (\text{S28})$$

We can write the diagonal bases in terms of the eigenvectors as

$$\begin{bmatrix} 1, & 0, & 0 \end{bmatrix} = \frac{v_+ + v_-}{\sqrt{2}}, \quad (\text{S29})$$

$$\begin{bmatrix} 0, & 1, & 0 \end{bmatrix} = \frac{1}{\sqrt{\Delta^2 + \Omega^2}} \left(\Delta \frac{v_+ - v_-}{\sqrt{2}} + \Omega v_0 \right), \quad (\text{S30})$$

$$\begin{bmatrix} 0, & 0, & 1 \end{bmatrix} = \frac{1}{\sqrt{\Delta^2 + \Omega^2}} \left(\Omega \frac{v_+ - v_-}{\sqrt{2}} - \Delta v_0 \right). \quad (\text{S31})$$

We can write the initial state for the $m_s = 0$ method as $\varphi_{110}(t=0) = [1, 1, 0]$, and for the $m_s = 1$ method by $\varphi_{001}(t=0) = [0, 0, 1]$. The time evolved states are then given by

$$\varphi_{110}(t) = \begin{bmatrix} \cos(\lambda t) - i \frac{\Delta \sin(\lambda t)}{\sqrt{\Delta^2 + \Omega^2}}, & \frac{\Delta^2 \cos(\lambda t) + \Omega^2}{\Delta^2 + \Omega^2} - i \frac{\Delta \sin(\lambda t)}{\sqrt{\Delta^2 + \Omega^2}}, & \frac{\Delta \Omega (\cos(\lambda t) - 1)}{\Delta^2 + \Omega^2} - i \frac{\Omega \sin(\lambda t)}{\sqrt{\Delta^2 + \Omega^2}} \end{bmatrix} \quad (\text{S32})$$

$$\varphi_{001}(t) = \begin{bmatrix} -i \frac{\Omega \sin(\lambda t)}{\sqrt{\Delta^2 + \Omega^2}}, & \frac{\Delta \Omega (\cos(\lambda t) - 1)}{\Delta^2 + \Omega^2}, & \frac{\Omega^2 \cos(\lambda t) + \Delta^2}{\Delta^2 + \Omega^2} \end{bmatrix}. \quad (\text{S33})$$

We note that the highest nuclear polarization is achieved for $\Omega = \pm\Delta$ at times

$$t_n = (2n + 1) \frac{\pi}{\sqrt{\Delta^2 + \Omega^2}}, \quad n = 0, 1, 2, 3, \dots \quad (\text{S34})$$

Note that, these conditions does not result in electronic spin polarization. However, as is shown in the main text we achieve electronic polarization at the end of the sequence for each method (See Figs. 4 and 5 of the main text). This is due to the optical excitation at the end of the sequence which allows the electronic spin to mainly polarize to $m_s = 0$ state while preserving the nuclear polarization.

ESLAC

In this section we give some details about the polarization based on the ESLAC method.

A. A_{ani} , A'_{\perp} components of the hyperfine interaction

In the ESLAC method, the polarization of the nuclear spin is achieved due to the A_{\perp} component of the hyperfine interaction (see Fig. 3(a) of the main text). However, the other components of the hyperfine interaction, i.e., A_{ani} and A'_{\perp} contribute to the depolarization of the nuclear spin. The anisotropic component causes precession between $|-1, \downarrow\rangle$ and $|-1, \uparrow\rangle$, between $|-1, \downarrow\rangle$ and $|0, \downarrow\rangle$, and between $|-1, \uparrow\rangle$ and $|0, \uparrow\rangle$. On the underhand, A'_{\perp} component causes precession between $|-1, \downarrow\rangle$ and $|0, \uparrow\rangle$. It can be seen in

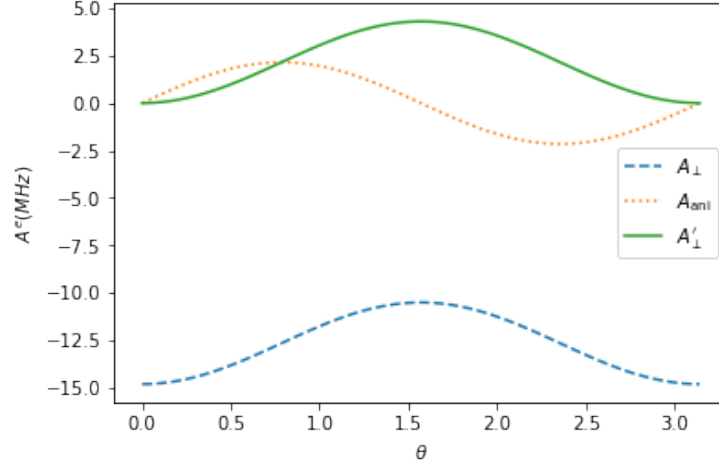


FIG. S1. Components of the excited state hyperfine matrix versus angle θ . The hyperfine matrix is constructed by calculating the contact term A_c , and dipole coupling A_d for a ^{13}C nuclear spin in family C setting $\varphi = 0$.

Fig. 6(e) of the main text that for the ESLAC method, the nuclear polarization decreases at angles close to $\theta = \pi/2$. For this range of θ , the A'_\perp component of the hyperfine interaction is larger. Figure S1 shows the components of the excited state hyperfine matrix for a carbon nuclear spin in family C. Setting the azimuthal angle to $\varphi = 0$, the contact term A_c and the dipole coupling A_d can be calculated as

$$A_c = (A_{xx} + A_{yy} + A_{zz})/3, \quad A_d = A_{xx} + A_{zz} - 2A_c. \quad (\text{S35})$$

The hyperfine matrix is then constructed for various angles θ using Eqs. (S6) to (S11).

B. Comparison with the experimental data for ^{15}N

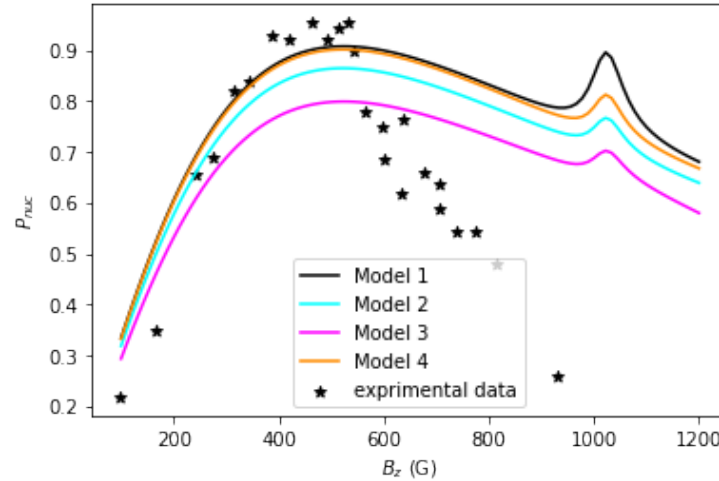


FIG. S2. ^{15}N nuclear polarization for ESLAC method versus B_z for all the 4 transition rate models given in the main text, Table 1. The experimental data (black stars) are taken from Ref. [S4].

We now compare our numerically simulated polarization for the ^{15}N using the ESLAC method with the experimental data of Ref. [S4]. Figure S2 shows the nuclear polarization versus magnetic field at steady state, i.e., for laser excitation time of 1ms. In this figure we have taken the electronic dephasing time for

the excited (ground) state to be $T_2^* = 6$ ns ($3\mu s$). Models 1 and 4 give the highest nuclear polarization. However, the simulated data is a little lower than the experimental data around $B \approx 520$ G. A higher nuclear polarization can be achieved by reducing the non-spin conserving transition rates, i.e., e in Table 1 of the main text, and increasing the ratio between the rates from the $m_s = 0$ and $m_s = \pm 1$ states to the singlet, i.e., $k_{\pm,S}/k_{0,S}$. For magnetic fields below the ESLAC, i.e., $B < 520$, our simulated data are consistent with the experimental data. However, for larger magnetic fields, our simulations in steady state give higher nuclear polarizations than the experimental data. This discrepancy may be due to some nuclear depolarization effects that we have not considered in our model.

C. Comparison with the experimental data

Here, we compare our results for the nuclear spin polarization achieved with the ESLAC method for ^{15}N and families A to H with the experimental data of Refs. [S4–S6]. As can be seen in Fig. S3(a), for ^{15}N and for families A to D our results are in good agreement with the experimental data. However, our simulated data result in a higher nuclear polarization for families E to H. This discrepancy could be due to the misalignment of the magnetic field in the experiments. In Fig. S3(b) we have shown that even for a small misaligned angle of 0.2 degrees for the magnetic field, the nuclear polarization reduces significantly for families C to H.

We note that we have taken the hyperfine matrix for such nuclear spin families from Ref. [S7]. The hyperfine matrix given in that reference is given in the principal axis system of the nuclear spin. The angle θ between the z axis of the nuclear spin, which is in the direction of the eigenvector corresponding to A_{zz} , and the z axis of the NV center is also given in that work. Setting the azimuthal angle, φ_H in the main text, to zero, a rotation around the y axis with angle θ gives the hyperfine matrix in the principal axis system of the NV [S8]. Note that, this angle θ is distinct from angle θ_H of the main text.

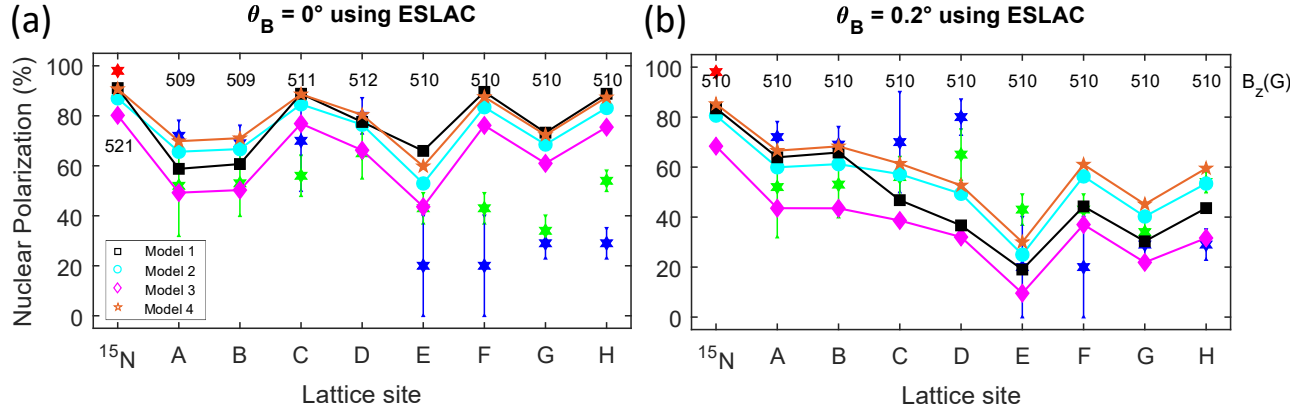


FIG. S3. Nuclear spin polarization for ^{15}N and ^{13}C families (A to H) for a magnetic field aligned with the NV axis, z axis (a) and for a magnetic field misaligned with the angle $\theta_B = 0.2$ degrees. The experimental data for ^{15}N (red star) is taken from Ref. [S4], and for ^{13}C families are taken from Refs. [S5] (blue stars) and [S6] (green stars).

SECOND ORDER CORRECTION

In this section we show how nonsecular terms of the Hamiltonian can be taken into account with second order perturbation theory. The Hamiltonian of the NV electron spin and a nuclear spin can be written as

$$H = DS_z^2 + \gamma_{el}\mathbf{B} \cdot \mathbf{S} + \gamma_n\mathbf{B} \cdot \mathbf{I} + \mathbf{S} \cdot \mathbf{A} \cdot \mathbf{I}, \quad (\text{S36})$$

where D is the zero field splitting, γ_{el} and γ_n are the gyromagnetic ratios of the electron and nuclear spin, \mathbf{A} is the hyperfine matrix and \mathbf{S} and \mathbf{I} are the electron and nuclear spin operators.

The secular terms of the above Hamiltonian can be written as

$$H_0 = DS_z^2 + \gamma_e B_z S_z + \gamma_n B_z I_z + \sum_j S_z A_{zj} I_j, \quad (\text{S37})$$

while the nonsecular terms are

$$V = \gamma_e B_x S_x + \gamma_e B_y S_y + \sum_j (S_x A_{xj} I_j + S_y A_{yj} I_j). \quad (\text{S38})$$

We take the nonsecular terms as a perturbation. Using the spin ladder operators S_\pm and defining $B_\pm = B_x \pm iB_y$ and $A_{j\pm} = A_{jx} \pm iA_{jy}$, the nonsecular terms can be written as

$$V = \frac{\gamma_e}{2} (S_+ B_- + S_- B_+) + \frac{1}{2} \sum_{j=x,y,z} (S_- A_{j+} + S_+ A_{j-}) I_j. \quad (\text{S39})$$

From the second order perturbation theory we have [S9]

$$E_n^{(2)} = \langle n^{(0)} | V \frac{\phi_n}{E_n^{(0)} - H_0} V | n^{(0)} \rangle, \quad (\text{S40})$$

where $|n^{(0)}\rangle$ are the eigenstates of the unperturbed Hamiltonian, H_0 , i.e., the eigenstates of S_z spin operator $|m_s\rangle$, and

$$\phi_n = 1 - |n^{(0)}\rangle \langle n^{(0)}| = \sum_{k \neq n} |k^{(0)}\rangle \langle k^{(0)}|. \quad (\text{S41})$$

Therefore, for $m_s = 0$ we obtain

$$E_{m_s=0}^{(2)} = \frac{\langle m_s = 0 | V | m_s = 1 \rangle \langle m_s = 1 | V | m_s = 0 \rangle}{E_0^{(0)} - E_1^{(0)}} + \frac{\langle m_s = 0 | V | m_s = -1 \rangle \langle m_s = -1 | V | m_s = 0 \rangle}{E_0^{(0)} - E_{-1}^{(0)}}. \quad (\text{S42})$$

where $E_0^{(0)} - E_{\pm 1}^{(0)} = -D \mp \gamma_e B_z$ and

$$\langle 0 | V | \pm 1 \rangle = \frac{1}{\sqrt{2}} \gamma_e B_\pm + \frac{1}{\sqrt{2}} \sum_j A_{j\pm} I_j, \quad (\text{S43})$$

$$\langle \pm 1 | V | 0 \rangle = \langle 0 | V | \pm 1 \rangle^*. \quad (\text{S44})$$

After some calculations we obtain

$$E_{m_s=0}^{(2)} = \frac{-2D\hat{M}}{2(D^2 - \gamma_e^2 B_z^2)} + \frac{2\gamma_e B_z \hat{N}}{2(D^2 - \gamma_e^2 B_z^2)}, \quad (\text{S45})$$

where we have defined

$$\hat{M} = 2\gamma_e [(A_{xx} B_x + A_{yx} B_y) I_x + (A_{xy} B_x + A_{yy} B_y) I_y + (A_{xz} B_x + A_{yz} B_y) I_z] + \gamma_e^2 B_\perp^2 \mathbf{1} + (\vec{A}_+ \cdot \vec{A}_-) \mathbf{1}, \quad (\text{S46})$$

$$\hat{N} = i(\vec{A}_+ \times \vec{A}_-) \cdot \vec{I}. \quad (\text{S47})$$

Here, $\mathbf{1}$ is the 2×2 identity matrix, and \vec{I} is a vector whose elements are the Pauli matrices $\vec{I} = (I_x, I_y, I_z)$. In the calculations we have used the following identity for Pauli matrices

$$(\vec{A}_+ \cdot \vec{I})(\vec{A}_- \cdot \vec{I}) = (\vec{A}_+ \cdot \vec{A}_-) \mathbf{1} + i(\vec{A}_+ \times \vec{A}_-) \cdot \vec{I}. \quad (\text{S48})$$

Similarly, for $m_s = \pm 1$ we have

$$E_{m_s=\pm 1}^{(2)} = \frac{\langle \pm 1 | V | 0 \rangle \langle 0 | V | \pm 1 \rangle}{E_{\pm 1}^{(0)} - E_0^{(0)}}, \quad (\text{S49})$$

which gives

$$E_{m_s=\pm 1}^{(2)} = \frac{\hat{M} \mp \hat{N}}{2(D \pm \gamma_e B_z)}. \quad (\text{S50})$$

To add the energies given in Eqs. (S45) and (S50) to the eigenenergies of the unperturbed Hamiltonian we add the following term to the unperturbed Hamiltonian, Eq. (S37),

$$H_{\text{soc}} = \frac{(3S_z^2 - 2)D + S_z \gamma_e B_z}{2(D^2 - \gamma_e^2 B_z^2)} \hat{M} + \frac{(2 - S_z^2) \gamma_e B_z - S_z D}{2(D^2 - \gamma_e^2 B_z^2)} \hat{N}. \quad (\text{S51})$$

The above equation is the second order correction term given in Eq. (8) of the main text.

-
- [S1] A. P. Nizovtsev, S. Ya Kilin, A. L. Pushkarchuk, V. A. Pushkarchuk, S. A. Kuten, O. A. Zhikol, S. Schmitt, T. Unden, and F. Jelezko, *New J. Phys.* **20** 023022 (2018).
- [S2] J. Preskill, “Quantum Information and Computation notes”, California Institute of Technology, 1998.
- [S3] T. Havel, *J. Math. Phys.* **44**, 534 (2003).
- [S4] V. Jacques, P. Neumann, J. Beck, M. Markham, D. Twitchen, J. Meijer, F. Kaiser, G. Balasubramanian, F. Jelezko, and J. Wrachtrup, *Phys. Rev. Lett.* **102**, 057403 (2009).
- [S5] B. Smeltzer, L. Childress, A. Gali, *New J. Phys.* **13**, 025021 (2011).
- [S6] A. Dréau, J. R. Maze, M. Lesik, J. F. Roch, and V. Jacques, *Phys. Rev. B* **85**, 134107 (2012).
- [S7] V. Ivády, K. Szász, A. L. Falk, P. V. Klimov, D. J. Christle, E. Jánzén, I. A. Abrikosov, D. D. Awschalom, and A. Gali, *Phys. Rev. B* **92** 115206 (2015).
- [S8] A. P. Nizovtsev, S. Y. Kilin, V. A. Pushkarchuk, A. L. Pushkarchuk, and S. A. Kuten, *Opt. Spectrosc.* **108**, 230 (2010).
- [S9] J. J. Sakurai, “Modern quantum mechanics”, Addison-Wesley Publishing (1994).